^{90}Y Radioembolization: Multimodality Imaging Pattern Approach with Angiographic Correlation for Optimized Target Therapy Delivery[1]

Juan C. Camacho, MD
Valeria Moncayo, MD
Nima Kokabi, MD
Hamilton E. Reavey, MD
James R. Galt, PhD
Kei Yamada, MD
Darren D. Kies, MD
Roger S. Williams, DO
Hyun S. Kim, MD
David M. Schuster, MD

Primary and metastatic liver cancers are responsible for considerable morbidity and mortality, and many patients are not curable at presentation. Therefore, new therapies such as radioembolization with yttrium 90 (^{90}Y)–labeled microspheres are an alternative method to treat patients with unresectable primary or secondary liver tumors. Patient selection, treatment technique, and early recognition of potential complications are the keys for successful patient outcomes. The activity of administered ^{90}Y microspheres depends on multiple variables, including the tumor burden, the volume of the liver lobe to be treated, the type of ^{90}Y microspheres, and the hepatopulmonary shunt fraction. Preprocedural planning relies on the results of cross-sectional imaging to determine the extent of disease, tumoral and nontumoral liver volumes, patency of the portal vein, and the degree of extrahepatic disease. A multidisciplinary approach that combines expertise in cross-sectional imaging, nuclear medicine, and flow dynamics is critical to adequately target malignant tissue. Preprocedural multimodality imaging, particularly combined single photon emission computed tomography (SPECT) and computed tomography (CT) imaging (SPECT/CT), may be used to identify nontarget imaging patterns that, if recognized, can potentially be corrected with either branch vessel embolization or catheter repositioning. Postprocedural multimodality imaging is also useful to confirm the appropriate delivery of ^{90}Y microspheres, enabling early identification of potential complications and the adequacy of microsphere distribution, thereby optimizing planning for subsequent therapies.

Abbreviations: FDG = fluorine 18 fluorodeoxyglucose, MAA = macroaggregates of human serum albumin

RadioGraphics 2015; 35:1602–1620

Published online 10.1148/rg.2015140314

Content Codes: GI IR NM OI VA

[1]From the Division of Interventional Radiology and Image-guided Medicine (J.C.C., N.K., K.Y., D.D.K., R.S.W.) and Division of Nuclear Medicine and Molecular Imaging (V.M., J.R.G., D.M.S.), Department of Radiology and Imaging Sciences, Emory University School of Medicine, 1364 Clifton Rd NE, Atlanta, GA 30322; Department of Radiology, Kaiser Permanente, Atlanta, Ga (H.E.R.); and Division of Interventional Radiology, Department of Radiology, University of Pittsburgh School of Medicine, Pittsburgh, Pa (H.S.K.). Presented as an education exhibit at the 2013 RSNA Annual Meeting. Received October 13, 2014; revision requested November 10 and received December 6; accepted December 11. For this journal-based SA-CME activity, the authors, editor, and reviewers have disclosed no relevant relationships. **Address correspondence to** J.C.C. (e-mail: *juan.camacho@emory.edu*).

See discussion on this article by Kalva and Sutphin (pp 1618–1620).

SA-CME LEARNING OBJECTIVES

After completing this journal-based SA-CME activity, participants will be able to:

- Explain the basic principles and indications for ^{90}Y radioembolization therapy.
- Identify the importance of preprocedural imaging, including cross-sectional, angiographic, and nuclear medicine examinations.
- Recognize the importance of pre- and postprocedural multimodality imaging patterns for adequate therapy planning and successful therapy delivery.

See www.rsna.org/education/search/RG.

Introduction

Yttrium 90 (^{90}Y) radioembolization therapy is a complex procedure that relies on the principle of intra-arterial brachytherapy and requires a multidisciplinary approach to ensure patient safety as a foundation to achieve favorable oncologic outcomes. In the appropriate clinical scenario, ^{90}Y radioembolization is a safe and effective therapy for patients presenting with primary and metastatic liver cancer (1–5). Several prospective randomized controlled trials are under way to assess, in comparison with other therapies, the clinical efficacies and benefits of administering intra-arterial brachytherapy in combination with other therapies and as the first-line therapy for primary and metastatic liver tumors.

TEACHING POINTS

- Yttrium 90 (^{90}Y) radioembolization therapy is a complex procedure that relies on the principle of intra-arterial brachytherapy and requires a multidisciplinary approach to ensure patient safety as a foundation to achieve favorable oncologic outcomes.
- Resin-based microspheres have a lower specific activity per particle and thus require more particles to achieve any given dose. Glass-based microspheres are routinely delivered as a complete dose with little embolic effect at a potentially greater dosage with larger parenchymal coverage.
- Preprocedural planning relies on cross-sectional imaging to determine the location and extent of disease. Ideally, three-phase computed tomographic (CT) or magnetic resonance (MR) imaging should be used to assess the tumoral and nontumoral liver volumes, the patency of the portal vein, and the degree of extrahepatic disease. Molecular imaging with positron emission tomography (PET) and CT (PET/CT) is useful to determine the metabolic tumoral volume in fluorine 18 fluorodeoxyglucose (FDG)–avid tumors and to establish baseline and follow-up response to therapy.
- The characteristics of MAA, specifically a particle size range of 10–90 μm, allow its use as a surrogate for ^{90}Y microsphere deposition into the hepatic arterial territory. If shunting or nontarget activity is identified, coil embolization or catheter repositioning at the time of therapy can be performed, or the therapy may be deferred. If this strategy is followed, potential complications, including gastrointestinal ulcers, pancreatitis, radiation-induced cholecystitis, and radiation pneumonitis, may be avoided.
- Interventional radiologists can optimize their therapeutic approach by using a multidisciplinary effort combining expertise in cross-sectional imaging, nuclear medicine, and flow dynamics to adequately target the patient's tumor burden. Complications may be avoided while optimizing tumor-directed therapy if proper imaging pattern recognition is pursued.

The purpose of this article is to describe the use of imaging in ^{90}Y radioembolization therapy for liver cancer. First, the general principles of ^{90}Y radioembolization therapy are described. Then the role of imaging for ^{90}Y radioembolization therapy is discussed. Finally, multimodality imaging patterns are related to ^{90}Y distribution.

General Principles of ^{90}Y Radioembolization Therapy

What Is ^{90}Y?

^{90}Y is the decay product of strontium 90 or may be produced by neutron bombardment of yttrium 89 (6). ^{90}Y is a pure beta-particle emitter, which decays to stable zirconium 90 (^{90}Zr) and has a physical half-life of 64.1 hours (2.67 days) (7). The average energy of beta-particle emissions is approximately 0.94 MeV (8). As a beta-particle emitter, ^{90}Y will induce cell death in surrounding tissue at the appropriate activity. One of the limitations of conventional radiation therapy in the treatment of liver tumors is the poor tolerance of the normal parenchyma to radiation. To destroy a solid tumor, a dose of at least 70 Gy is required to cause irreversible cellular damage, yet the hepatic parenchymal tolerance level is closer to 30–40 Gy. At a dose of 40 Gy, the chance of causing radiation-induced liver damage is approximately 50% (9,10). Because most hepatic malignancies are radiosensitive and have predominant arterial inflow rather than portal venous supply (11), ^{90}Y microspheres concentrate within tumors, inducing radiation cell death with relative sparing of the uninvolved liver parenchyma (7,12).

Vehicles Delivering ^{90}Y: Resin and Glass Microspheres

Two different ^{90}Y products are available in the United States: glass microspheres (13) and resin microspheres (14). Glass microspheres (TheraSphere; BTG, London, England) are insoluble particles with a mean diameter of 20–30 μm (compared with 20–60 μm for the resin microspheres) (7). In the glass microsphere product, ^{90}Y is incorporated into the glass matrix, whereas in the resin microspheres (SIR-Spheres; Sirtex Medical, North Sydney, Australia), the radioisotope is bound to the surface of the resin microsphere. Other important differences between the glass microsphere and the resin microsphere include the specific gravity (3.6 vs 1.6 g/dL, respectively), the activity per microsphere (150–2200 Bq vs 65–140 Bq, respectively), and the number of microspheres per vial ($1.2–8 \times 10^6$ vs $40–80 \times 10^6$, respectively) (7,12,15).

Resin-based microspheres have a lower specific activity per particle and thus require more particles to achieve any given dose. Glass-based microspheres are routinely delivered as a complete dose with little embolic effect at a potentially greater dosage with larger parenchymal coverage (16,17). No direct comparison of the efficacy of the two microsphere products has been reported in the literature.

Although the specific activity per microsphere is typically greater with glass microspheres, compared with resin microspheres, the ^{90}Y glass microspheres may be allowed to decay for a greater period of time before the treatment session (approximately 2 weeks vs 1 week), which will result in a lower specific activity per glass microsphere. In this situation, a larger starting dose for the glass microspheres at production will then result in a substantially increased number of glass microspheres per dose (up to 30×10^6), enabling greater theoretic parenchymal coverage and allowing a greater embolic dose (18).

Indications and Contraindications for ^{90}Y Therapy

The findings from numerous studies have demonstrated that a substantial benefit results from

providing intra-arterial therapies for liver tumors (1,2,4,5,7,13,19,20). Radioembolization and the integration of combination therapies have improved response rates and the survival of patients with liver neoplasms (21–24).

Indications for ^{90}Y radioembolization include management of primary liver malignancies (including hepatocellular carcinoma and cholangiocarcinoma), as well as metastatic disease to the liver parenchyma (8,13,14). The Food and Drug Administration–approved indication for the resin microspheres is treatment of unresectable hepatic metastases from colorectal cancer with adjuvant intrahepatic arterial chemotherapy of floxuridine. Glass microspheres are approved with a humanitarian device exemption (HDE) as neoadjuvant therapy to surgery or transplantation in patients with unresectable hepatocellular carcinoma. However, the therapies are often administered for off-label use or with an extension of indications in the HDE. Objectives of ^{90}Y therapy include "downstaging" neoplastic liver disease, prolonging recurrence-free and overall survival, and bridging patients to transplantation or resection (1,3–5,13,19,25).

According to the consensus panel report from the Radioembolization Brachytherapy Oncology Consortium, patients considered for radioembolization therapy include those with *(a)* unresectable hepatic primary or metastatic cancer, *(b)* liver-dominant tumor burden, and *(c)* life expectancy of at least 3 months as part of multidisciplinary palliative care (26).

Contraindications for microsphere radioembolization therapy include *(a)* deposition of technetium 99m (^{99m}Tc)–labeled macroaggregates of human serum albumin (MAA) in the gastrointestinal tract that is not correctable with angiographic techniques; *(b)* shunting to the lungs that could result in delivery of more than 30 Gy to the pulmonary parenchyma in a single treatment and more than 50 Gy as a cumulative dose; *(c)* contraindications to hepatic artery catheterization, including technical difficulties or bleeding diathesis; *(d)* severe liver dysfunction or pulmonary insufficiency; or *(e)* main portal vein thrombosis (although treatment can be considered on a case-by-case basis) (18). Caution is also advised in patients who exhibit *(a)* a bilirubin level of 1.5 mg/dL or more (unless superselective embolization can be performed) and *(b)* an extensive tumor burden with limited hepatic reserve and specific abnormal results of liver function tests (18). Patients who have undergone prior radiation therapy involving the liver should also be carefully reviewed on a case-by-case basis to ensure that adequate hepatic function is maintained after therapy. Additional warning is advised for patients with an Eastern Cooperative Oncology Group (ECOG) performance score greater than 1.

Role of Imaging for ^{90}Y Microsphere Therapy

Preprocedural Cross-sectional Imaging and Patient Evaluation

The amount of ^{90}Y activity administered to a patient depends on multiple variables, including the tumor burden, the absolute or relative volume of liver to be treated, the type of ^{90}Y microsphere (ie, glass or resin), and the hepatopulmonary shunt fraction. Preprocedural planning relies on cross-sectional imaging to determine the location and extent of disease.

Ideally, three-phase computed tomographic (CT) or magnetic resonance (MR) imaging should be used to assess the tumoral and nontumoral liver volumes, the patency of the portal vein, and the degree of extrahepatic disease. Molecular imaging with positron emission tomography (PET) and CT (PET/CT) is useful to determine the metabolic tumoral volume in fluorine 18 fluorodeoxyglucose (FDG)–avid tumors and to establish baseline and follow-up response to therapy (27–29).

Furthermore, the hepatic and biochemical status of each patient should be evaluated to ensure that the patient demonstrates adequate liver function to undergo microsphere therapy. Satisfactory renal function to allow angiographic examination, as well as overall good functional status before ^{90}Y radioembolization, is crucial for favorable patient outcomes (26,30,31).

Combined Preprocedural Angiographic Vascular Mapping and ^{99m}Tc-MAA Shunt Examination

Suitable patients should undergo a ^{99m}Tc-MAA shunt examination, which offers important preprocedural information (32). Variant hepatic arterial anatomy occurs commonly and has been reported in 25%–45% of the individuals in large surgical series (33,34). Conventional hepatic arteries are supplied through the celiac trunk and arise from the proper hepatic artery, which in turn arises from the common hepatic artery, distal to the gastroduodenal origin (Fig 1). Given the propensity for arterial variants and the development of hepatopulmonary shunting in hepatic tumors, careful consideration of the dose delivery point is crucial for optimal coverage of target lesions.

Selective angiography of the superior mesenteric artery should be performed to exclude replaced or accessory hepatic arteries arising from the superior mesenteric artery. Failure to identify

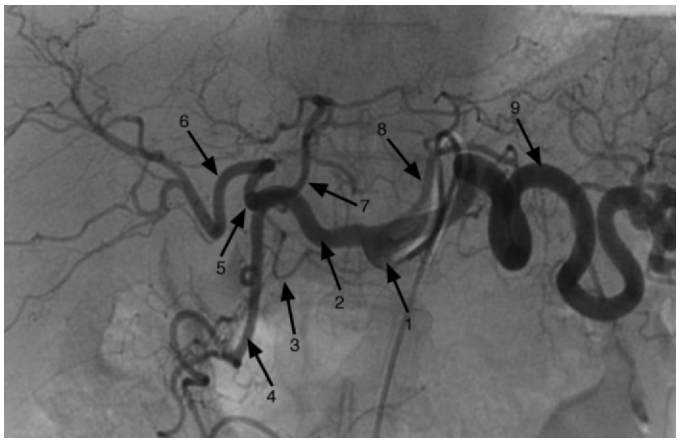

Figure 1. Conventional celiac anatomy. Celiac axis angiogram shows conventional hepatic arterial anatomic structures. *1* = celiac axis, *2* = common hepatic artery, *3* = right gastric artery, *4* = gastroduodenal artery, *5* = proper hepatic artery, *6* = right hepatic artery, *7* = left hepatic artery, *8* = left gastric artery, *9* = splenic artery.

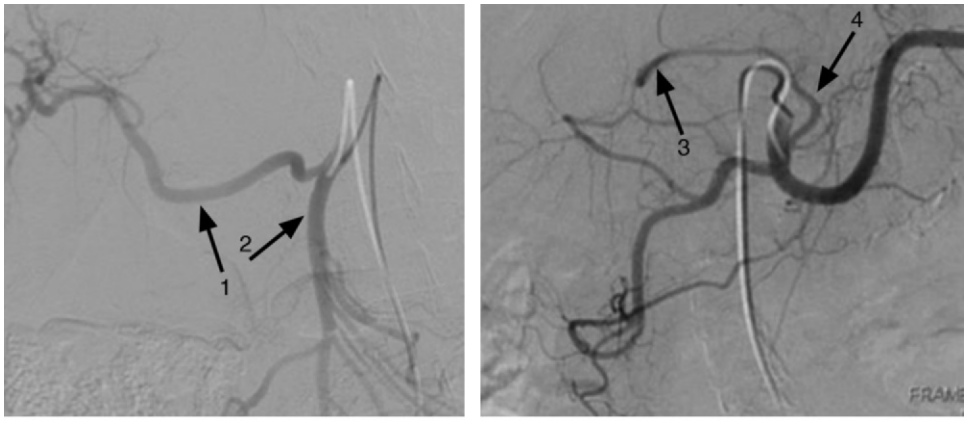

a. **b.**

Figure 2. Common anatomic variants that may predispose to nontarget embolization. **(a)** Digital subtraction angiogram shows a replaced right hepatic artery *(1)* from the superior mesenteric artery *(2)*. **(b)** Digital subtraction angiogram shows an accessory left hepatic artery *(3)* from the left gastric artery *(4)*.

a replaced or accessory hepatic arterial supply could have important implications for proper estimation of the hepatopulmonary shunt fraction and for complete targeted delivery to the liver tumor (Fig 2).

To avoid extrahepatic nontarget embolization of surrounding organs, accurate superselective angiographic evaluation of the targeted vascular territory should be performed, which includes prophylactic embolization of nonhepatic branch vessels during the mapping examination (35). Some potential nonhepatic branch vessels arise directly from the right or left hepatic arteries and must be embolized to safely administer ^{90}Y microspheres. For example, the right gastric artery often arises as the first branch of the left hepatic artery. Additionally, accessory left gastric or inferior phrenic arteries can also arise from the left hepatic artery and may be difficult to identify. Other nonhepatic branch vessels, particularly the gastroduodenal artery, arise proximal to the usual intended point of ^{90}Y microsphere infusion. If there is concern for arterial reflux and nontarget embolization due to anatomic variants or extrahepatic vessels arising within the treatment territory, prophylactic embolization can be performed (36–38). When performing imaging of the left hepatic artery, two considerations should be taken into account: *(a)* It is important to try to determine the origin of the umbilical artery, which can potentially be a source of nontarget embolization. *(b)* When imaging segment IV arteries, it is important to determine if there are appreciable cross-filling arteries. Both of these factors can lead to unintended nontarget embolization.

After microcatheter placement at the origin of the target hepatic territory, a dose of 148 MBq (4 mCi) of ^{99m}Tc-MAA is usually administered (39). Whole-liver or more selective administration of ^{99m}Tc-MAA may be performed, depending on the anatomic distribution of the tumor as well as institutional preference. Although ideally a selective MAA examination may be useful before each session of planned ^{90}Y therapy in the same vascular distribution, a single ^{99m}Tc-MAA whole-liver examination is commonly performed to spare the patient the cost and potential morbidity of an additional procedure. This examination may be

accomplished either with a single proper hepatic artery administration or with divided lobar doses.

The characteristics of MAA, specifically a particle size range of 10–90 μm, allow its use as a surrogate for ^{90}Y microsphere deposition into the hepatic arterial territory (40). If shunting or nontarget activity is identified, coil embolization or catheter repositioning at the time of therapy can be performed, or the therapy may be deferred. If this strategy is followed, potential complications, including gastrointestinal ulcers, pancreatitis, radiation-induced cholecystitis, and radiation pneumonitis, may be avoided (7,41–44).

^{99m}Tc-MAA planar imaging of the thorax and abdomen and an optional hybrid examination with single photon emission computed tomography (SPECT) and CT (SPECT/CT) are then performed within 1 hour after intraarterial ^{99m}Tc-MAA administration to determine the hepatopulmonary shunt fraction (26). It is preferable to image as close as possible to the injection time to avoid false-positive extrahepatic activity caused by free technetium (26). Images are obtained by using a gamma camera with a large field of view, with a low-energy high-resolution parallel hole collimator and a 15% or 20% window centered at 140 keV. In addition, a cobalt 57 transmission source may be useful with planar imaging to outline the body as an aid in positioning. Although SPECT/CT is an optional component of this examination, various investigators have suggested that ^{99m}Tc-MAA SPECT/CT could disclose potential nontarget areas of embolization not identified at angiography (45–48). If SPECT/CT is not available, SPECT may be useful instead. It has been our experience that SPECT/CT adds valuable preprocedural information to adequately target the tumor.

Patients with a hepatic shunt fraction of greater than 20% are generally not ideal candidates for ^{90}Y radioembolization because of an increased risk of developing radiation pneumonitis, although the therapy may still be administered in individual cases if the total activity delivered to the lungs will be less than the recommended thresholds of 30 Gy per treatment session and 50 Gy for the cumulative dose (Fig 3). However, the decreased dose required to spare the lungs with shunts of more than 20% often makes the therapy suboptimal or ineffective.

Additional angiographic techniques such as cone-beam CT have been recently incorporated into routine clinical practice at some centers to minimize procedural risks and to avoid nontarget embolization. Incorporation of cone-beam CT during the ^{99m}Tc-MAA shunt examination session allows detection and exclusion of extrahepatic enhancement more precisely than conventional angiography, increasing the specificity and negative predictive values of the ^{99m}Tc-MAA shunt examination and potentially decreasing the risk of therapy-induced complications (49,50). Cone-beam CT also provides detailed information about tumor vascularity and tumoral vascular supply and, in more than one-half of the patients, allows identification of extrahepatic tumoral vascular supply when compared with conventional angiography alone (51,52).

The availability of an advanced multimodality workstation will enable fusion of the ^{99m}Tc-MAA SPECT images to images obtained with other modalities, such as PET/CT or MR imaging, although accurate registration may be difficult because the ^{99m}Tc-MAA is confined to the liver and provides few anatomic landmarks. If the examination is performed on a SPECT/CT platform, the acquired CT examination may be used as a "vehicle" to first perform anatomic fusion and thus coregister the functional ^{99m}Tc-MAA images to MR images or to molecular images such as PET/CT images.

^{90}Y Microsphere Dose Calculation

The administered activity for each patient is calculated on the basis of the type of microsphere used. On the basis of the manufacturer's recommendations and published guidelines, the glass microsphere activity required (AR) (in gigabecquerels) is calculated by using the following formula, which incorporates the target desired dose (DD) (in gray), the mass of liver to be treated ($mass_{liver}$) (in kilograms), the lung shunt fraction (LSF), and the anticipated residual waste *(R)* (13):

$$AR = (DD \times mass_{liver})/[50 \times (1 - LSF) \times (1 - R)].$$

Target dose is typically 120 Gy (range, 80–150 Gy). The mass of the liver lobe to be treated is estimated by calculating the lobe volume with the use of three-dimensional rendering medical imaging software, assuming 1.03 g/cm^3 of liver tissue. With bilobar hepatic involvement, ^{90}Y microsphere therapy is commonly administered in lobar doses, rather than to the entire liver, to ensure adequate hepatic reserve.

Take the example of a patient who has received no prior ^{90}Y microsphere therapy, with an 1800-cm^3 total liver volume, a 5% lung shunt fraction, and 1% anticipated residual waste, who will receive a 120-Gy desired dose to the 1000-cm^3 (1.03-kg) right lobe. For this patient, the required activity (RA) (in gigabecquerels) is calculated as follows: RA = (120 × 1.03)/[(50 × (1 − 0.05) × (1 − 0.01)]. A dose of 2.63 GBq is thus required at administration.

The calculation of administered activity for resin-based microspheres may be performed with two different methods. The method recommended by the manufacturer uses body surface

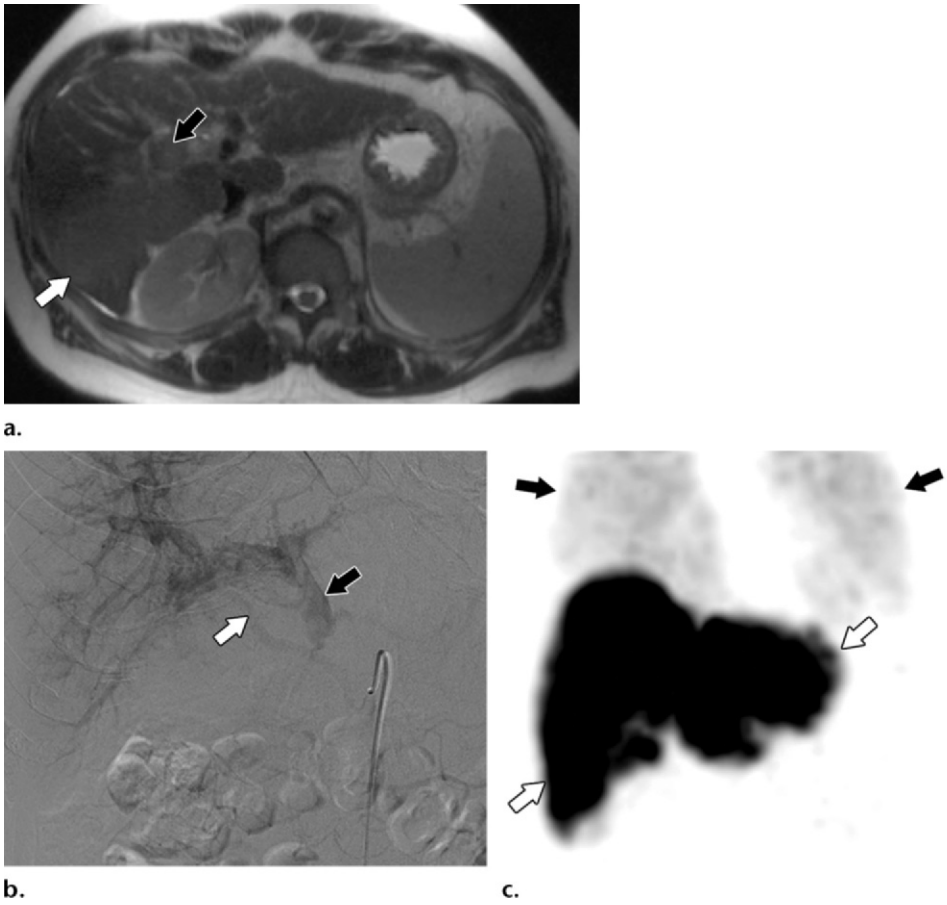

Figure 3. Importance of performing a ^{99m}Tc-MAA shunt examination. A 59-year-old man presented with infiltrative hepatocellular carcinoma with macrovascular invasion and no extrahepatic disease. **(a)** Axial T2-weighted MR image of the liver shows a geographic area of high T2 signal intensity (white arrow) involving the posterior segment of the right liver lobe. This finding is associated with an expanded right portal vein (black arrow), which shows similar signal intensity characteristics when compared with the involved liver lobe; therefore, the findings correspond to an infiltrative hepatocellular carcinoma with lobar portal vein tumoral thrombosis. **(b)** Angiogram obtained before the ^{99m}Tc-MAA examination shows catheter placement in the superior mesenteric artery (because of a replaced right hepatic artery); and while in the arterial phase, there is opacification of the common hepatic artery (white arrow) with early opacification of the main portal vein, including the intrahepatic branches, because of high flow shunting during the administration of contrast material (black arrow). **(c)** ^{99m}Tc-MAA maximum intensity projection image shows tracer activity throughout the right and left hepatic lobes (white arrows) (despite a replaced right hepatic artery injection), as well as in both lungs (black arrows), because of extensive portal shunting. The lung shunt fraction in this particular case corresponded to 55%, and the ^{90}Y radioembolization therapy was subsequently cancelled.

area (BSA) as a proxy for the liver volume of the patient to calculate the prescribed activity (in gigabecquerels) in the following way (53): activity = (BSA − 0.2) + (% tumor involvement of liver/100).

For lobar therapy, the activity is then multiplied by the lobar mass as a fraction of the entire liver. Various reduction factors are also applied, including activity reduction for abnormal results of liver function tests, small tumor load, and prior radiation therapy.

Thus, for the same hypothetical patient described in the preceding paragraphs who is receiving right lobe therapy, the body surface area and the percent tumor involvement would be used for the calculation of prescribed activity (in gigabecquerels); for example, 2.03 and 20%, respectively: activity = (2.03 − 0.2) + (20/100). This calculation would result in 2.03 GBq required for the entire liver, which is then multiplied by the 55.6% right lobar mass to yield a 1.13-GBq dose required at therapy.

A second empirical method to calculate prescribed activity for resin-based microspheres uses the percentage of liver involvement by the tumor to determine the starting activity and is modified by a lung shunt modifier and a liver part modifier (26).

More sophisticated planning methods have also been advocated in an attempt to provide greater individualization and dosimetric activity calculations (54–58).

Therapy Administration: Consolidation of Multidisciplinary Effort

Multiple safety procedures are carried out on the day of therapy in an effort to control variables that may interfere with therapy delivery, including *(a)* verification of pregnancy status, if applicable, *(b)* confirmation of dose calculations and the liver lobe to be treated, and *(c)* preparation of the angiography suite to comply with additional radioisotope safety measurements. In our facility, a running checklist is completed, and nuclear medicine personnel visit the patient in the holding area to review radiation safety precautions. The interventional radiologist then administers the therapy with the assistance of the multidisciplinary team.

Postprocedural Bremsstrahlung Examination

The beta particles emitted by ^{90}Y produce secondary bremsstrahlung radiation, which may be imaged to document ^{90}Y microsphere deposition. Bremsstrahlung radiation is caused by the beta particle losing energy as it passes close to the atomic nucleus. A postprocedural ^{90}Y bremsstrahlung planar or SPECT/CT scan is helpful after treatment to evaluate actual posttherapy microsphere distribution and to identify radiotracer activity outside the tumoral coverage areas. The use of SPECT/CT increases the sensitivity of detecting extrahepatic activity (7,41–43,59,60). Imaging patterns that are based on our experience with pre- and posttherapy multimodality imaging are described in the following paragraphs.

Planar and SPECT bremsstrahlung imaging of the abdomen may be performed by using medium-energy high-resolution parallel hole collimation. Unlike the monoenergetic radiation produced by the radionuclides commonly used for nuclear imaging, bremsstrahlung radiation is a continuous spectrum with a maximum energy equal to that of the beta particle (0.94 MeV) and presents unique problems for imaging. Although consensus has not been reached on the optimum energy window for imaging, a 30% energy window centered at 75 keV or a 32% window centered at 108 keV is often used. It should be noted that if the gamma camera auto-peaks on acquisition, this feature should be turned off because the lack of a well-defined energy peak may produce unpredictable results. The bremsstrahlung images from separate therapies may be coregistered to each other or to images from other modalities to ensure adequate therapy coverage (Fig 4).

The 0+/0+ transition of ^{90}Zr, which results in a $\beta+/\beta-$ pair creation, provides the opportunity to detect ^{90}Y distribution by using PET (22). Clinical applications of PET imaging with ^{90}Y have been reported recently in the context of radioembolization, radioimmunotherapy for lymphoma, and peptide receptor radionuclide therapy (61–65). ^{90}Y bremsstrahlung imaging with SPECT/CT demonstrates low spatial resolution; therefore, imaging with PET/CT may be beneficial for small foci of activity. In addition, quantification of delivered activity to lesions may be more accurate with PET, compared with SPECT. Disadvantages associated with PET imaging are low counts and longer imaging time, as well as greater economic cost (66).

Multimodality Imaging Patterns: Classification to Improve Targeted Therapy

Interventional radiologists can optimize their therapeutic approach by using a multidisciplinary effort combining expertise in cross-sectional imaging, nuclear medicine, and flow dynamics to adequately target the patient's tumor burden. Complications may be avoided while optimizing tumor-directed therapy if proper imaging pattern recognition is pursued.

Multimodality Imaging Approach

Multimodality SPECT/CT or PET/CT allows the categorization of patients into those with target and nontarget ^{90}Y distributions. Both pretherapy ^{99m}Tc-MAA and posttherapy bremsstrahlung imaging (or PET/CT) can be used in an iterative manner. Pretherapy multimodality imaging will inform the approach to therapy, which can then be evaluated with posttherapy imaging, which in turn may be used to direct subsequent treatment.

Multimodality imaging may demonstrate target and nontarget ^{90}Y microsphere distribution, as well as complete or incomplete tumoral coverage (Fig 5). If the distribution of the ^{90}Y microspheres is to the appropriate target, complete or incomplete lesion coverage by the radioisotope can be identified. When a nontarget distribution is observed as an imaging pattern, the distribution may be extrahepatic (ie, stomach, duodenum, gallbladder, or other visceral structure) or intrahepatic (ie, intrahepatic reflux, intrahepatic shunting at the capillary level, or nontarget vessel flow redistribution).

As demonstrated in the following sections, incomplete lesion coverage and/or nontarget distribution, if recognized at pretherapy imaging, may be avoided by *(a)* modification of therapy delivery by using catheter repositioning techniques or pretherapy branch vessel embolization or *(b)* withholding targeted therapy. However, sometimes nontarget ^{90}Y microsphere distribution or incomplete target coverage is unexpected

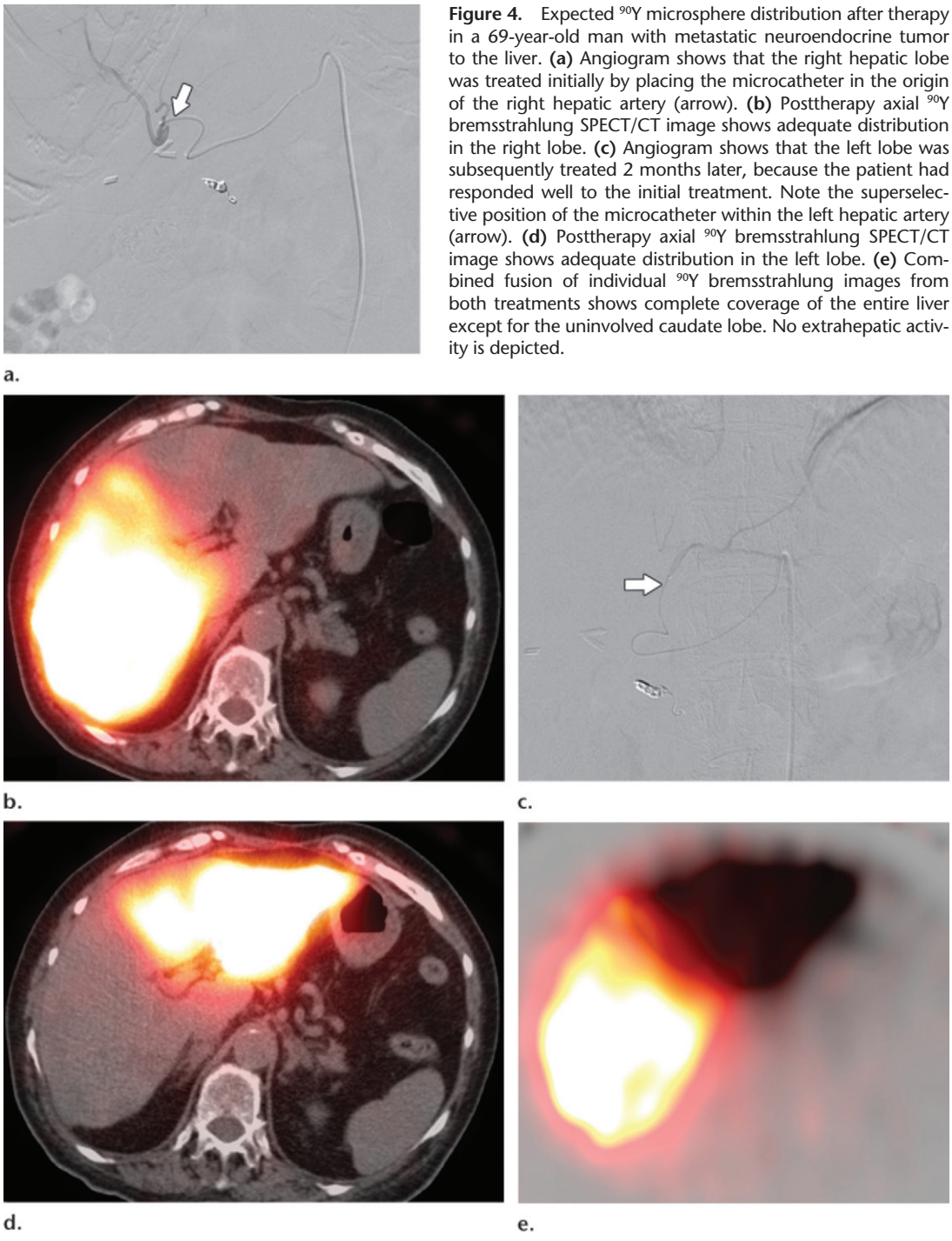

Figure 4. Expected ^{90}Y microsphere distribution after therapy in a 69-year-old man with metastatic neuroendocrine tumor to the liver. **(a)** Angiogram shows that the right hepatic lobe was treated initially by placing the microcatheter in the origin of the right hepatic artery (arrow). **(b)** Posttherapy axial ^{90}Y bremsstrahlung SPECT/CT image shows adequate distribution in the right lobe. **(c)** Angiogram shows that the left lobe was subsequently treated 2 months later, because the patient had responded well to the initial treatment. Note the superselective position of the microcatheter within the left hepatic artery (arrow). **(d)** Posttherapy axial ^{90}Y bremsstrahlung SPECT/CT image shows adequate distribution in the left lobe. **(e)** Combined fusion of individual ^{90}Y bremsstrahlung images from both treatments shows complete coverage of the entire liver except for the uninvolved caudate lobe. No extrahepatic activity is depicted.

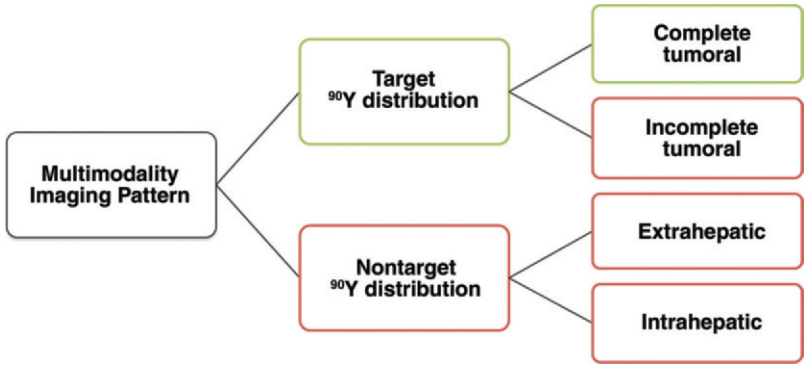

Figure 5. Diagram summarizing the different multimodality imaging uptake patterns. The goal is target ^{90}Y microsphere distribution with complete tumoral coverage.

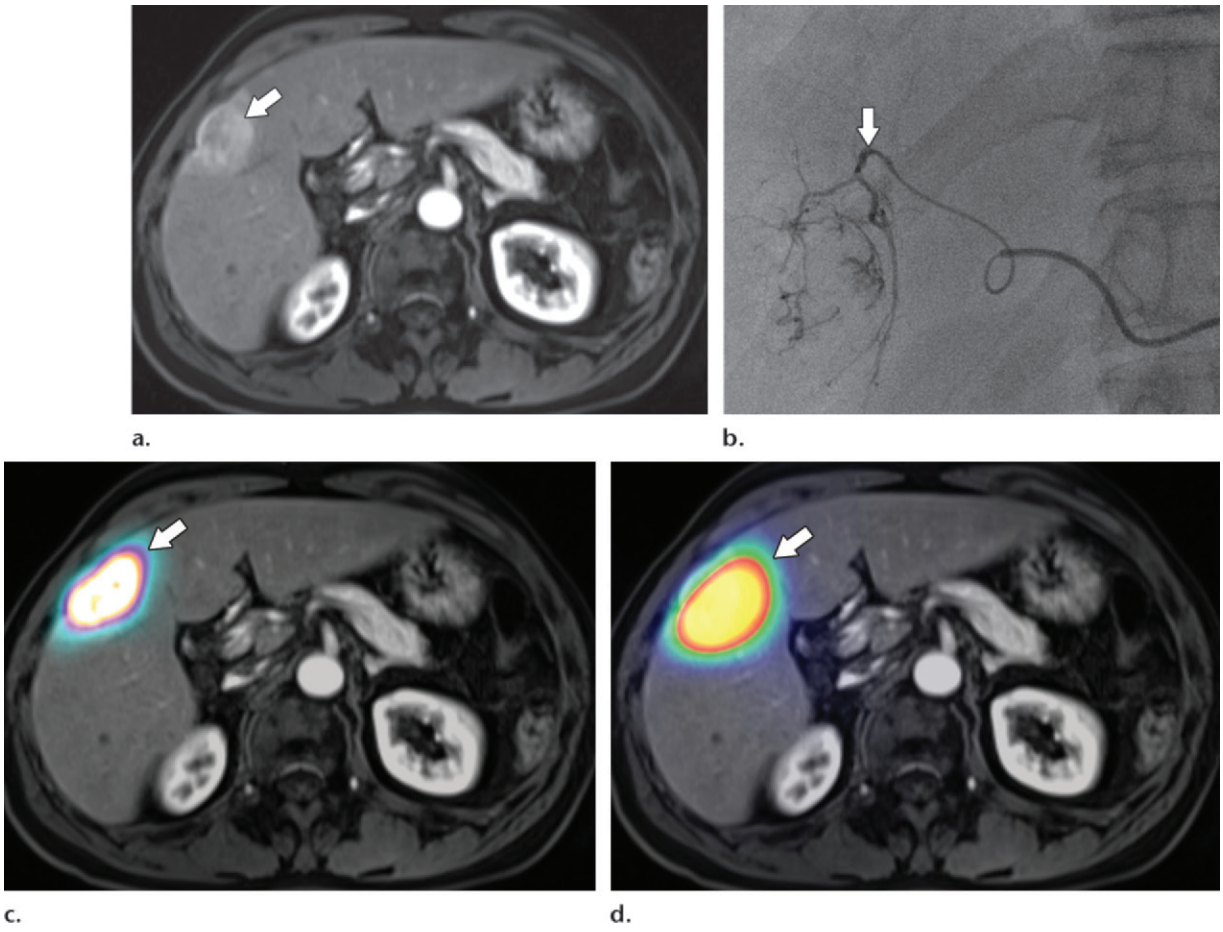

Figure 6. Target distribution with intratumoral pattern. Images of a 69-year-old man with hepatocellular carcinoma show ^{90}Y microsphere target distribution, with complete tumoral distribution at pretherapy evaluation, as well as at posttherapy imaging. **(a)** Axial contrast-enhanced T1-weighted MR image (arterial phase) shows an arterially enhancing lesion (arrow) within segment V of the liver parenchyma, a finding that corresponds to a hepatocellular carcinoma. **(b)** Selective angiogram of the anterior branch of the right hepatic artery shows adequate catheter position (arrow) for ^{99m}Tc-MAA delivery. **(c)** Coregistered ^{99m}Tc-MAA SPECT/CT and MR image shows complete tumoral distribution of the ^{99m}Tc-MAA (arrow). **(d)** Coregistered posttherapy ^{90}Y bremsstrahlung and pretherapy MR image also shows complete tumoral distribution of the therapy (arrow).

or unavoidable but can be identified at posttherapy multimodality imaging, allowing immediate intervention or mitigation by altering the subsequent approach.

Target ^{90}Y Distribution: Complete and Incomplete Imaging Patterns

Complete tumoral coverage refers to the administration of the microspheres into the tumoral territory (Fig 6). Given the arterial dominant supply of most tumors, complete tumoral distribution is expected. However, incomplete distribution may occur because of flow dynamics or, possibly, operator error. When incomplete distribution is identified, the operator may be able to correct the catheter position for a more targeted complete therapy delivery (Fig 7). Additionally, coil embolization of nonhepatic vessels (ie, phrenic artery) increases the flow to the liver by increasing the resistance of blood flow in nontarget territories and, therefore, increases the likelihood of target therapy delivery. Ideally, pre- and posttherapy multimodality imaging may be used in an iterative fashion to deliver optimized care (Fig 8). However, substantial incomplete tumoral coverage may reflect poor arterial supply of the target lesion and may also be an indication of extrahepatic vessel parasitization. Although this incomplete distribution may be partially mitigated, complete tumoral coverage may not be possible. This imaging pattern may explain why this type of lesion can demonstrate a suboptimal response to microsphere therapy.

Nontarget ^{90}Y Distribution: Intrahepatic and Extrahepatic Imaging Patterns

Nontarget embolization may be intrahepatic or extrahepatic. If nontarget embolization is seen at pretherapy imaging, catheter redirection may then result in optimal therapy. Both target incomplete and nontarget intrahepatic patterns may coexist in the same imaging session (Fig 7d). The

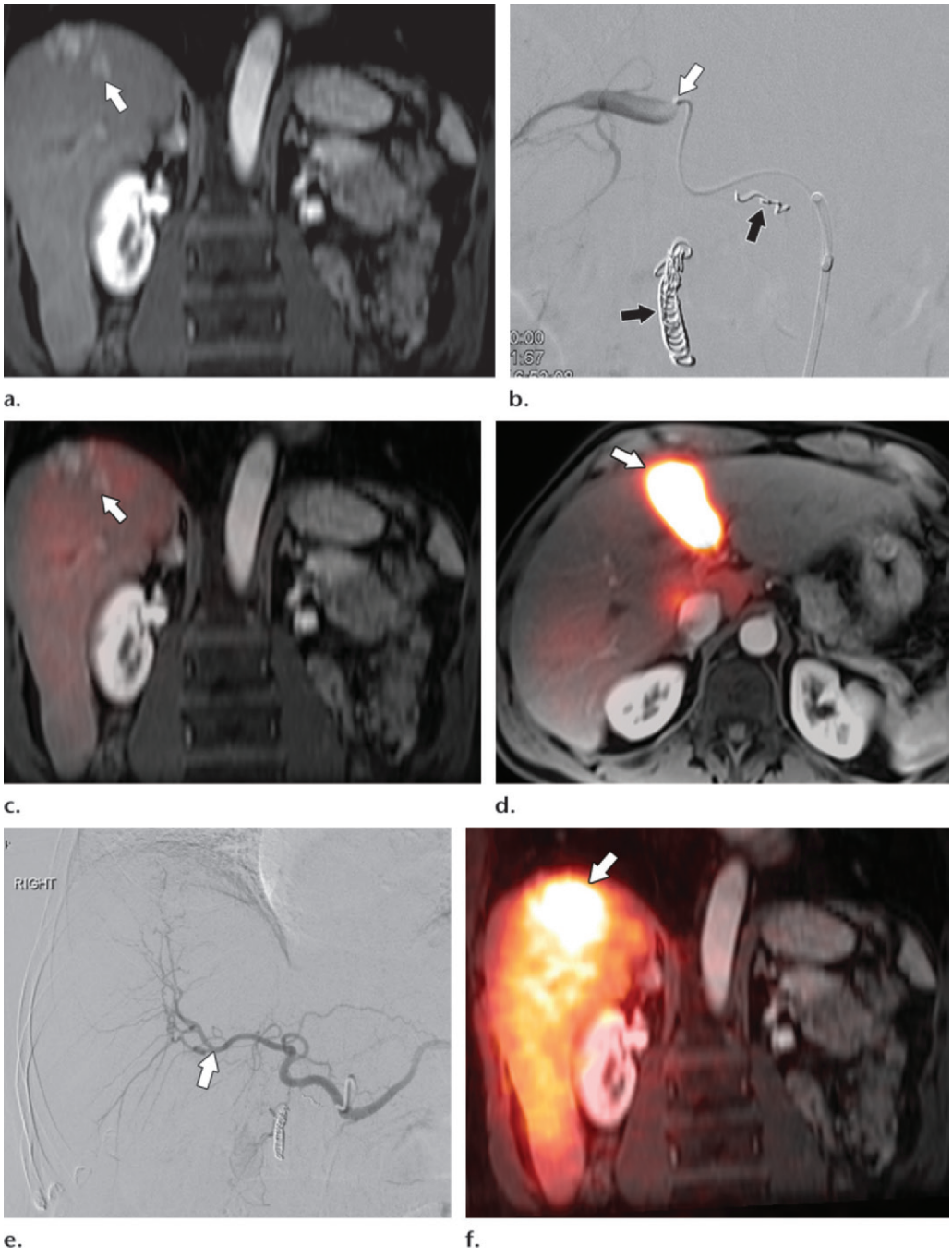

Figure 7. Incomplete tumoral and nontarget intrahepatic distribution, which was corrected to target complete tumoral distribution. Images of a 52-year-old man with multifocal hepatocellular carcinoma show intrahepatic nontarget particle redistribution at initial ^{99m}Tc-MAA SPECT/CT, a finding that was corrected at subsequent therapy with angiographic adjustment. **(a)** Coronal contrast-enhanced T1-weighted MR image (arterial phase) shows multiple foci of arterial enhancement (arrow) within segment VII/VIII of the liver parenchyma, a finding that corresponds to multifocal hepatocellular carcinoma. **(b)** Selective angiogram of the right hepatic artery just beyond the vessel bifurcation (white arrow) shows adequate catheter position for ^{99m}Tc-MAA delivery. Note prior coil embolization of the right gastric and the gastroduodenal arteries (black arrows). **(c)** Coregistered coronal ^{99m}Tc-MAA SPECT/CT shunt and preprocedural MR image shows minimal radiotracer activity within the right lobe and minimal intratumoral distribution within the target lesions (arrow). **(d)** Coregistered axial ^{99m}Tc-MAA SPECT/CT and pretherapy MR image shows ^{99m}Tc-MAA distribution predominantly within segment IV of the liver parenchyma (arrow). **(e)** Subsequent selective angiogram obtained at the time of therapy allowed identification of the proximal segment IV branch stealing the majority of flow; therefore, the microcatheter was repositioned during therapy delivery and advanced into the superior division of the right hepatic artery (arrow). **(f)** Coregistered coronal ^{90}Y bremsstrahlung and pretherapy MR image shows the now complete tumoral distribution of the ^{90}Y microspheres (arrow).

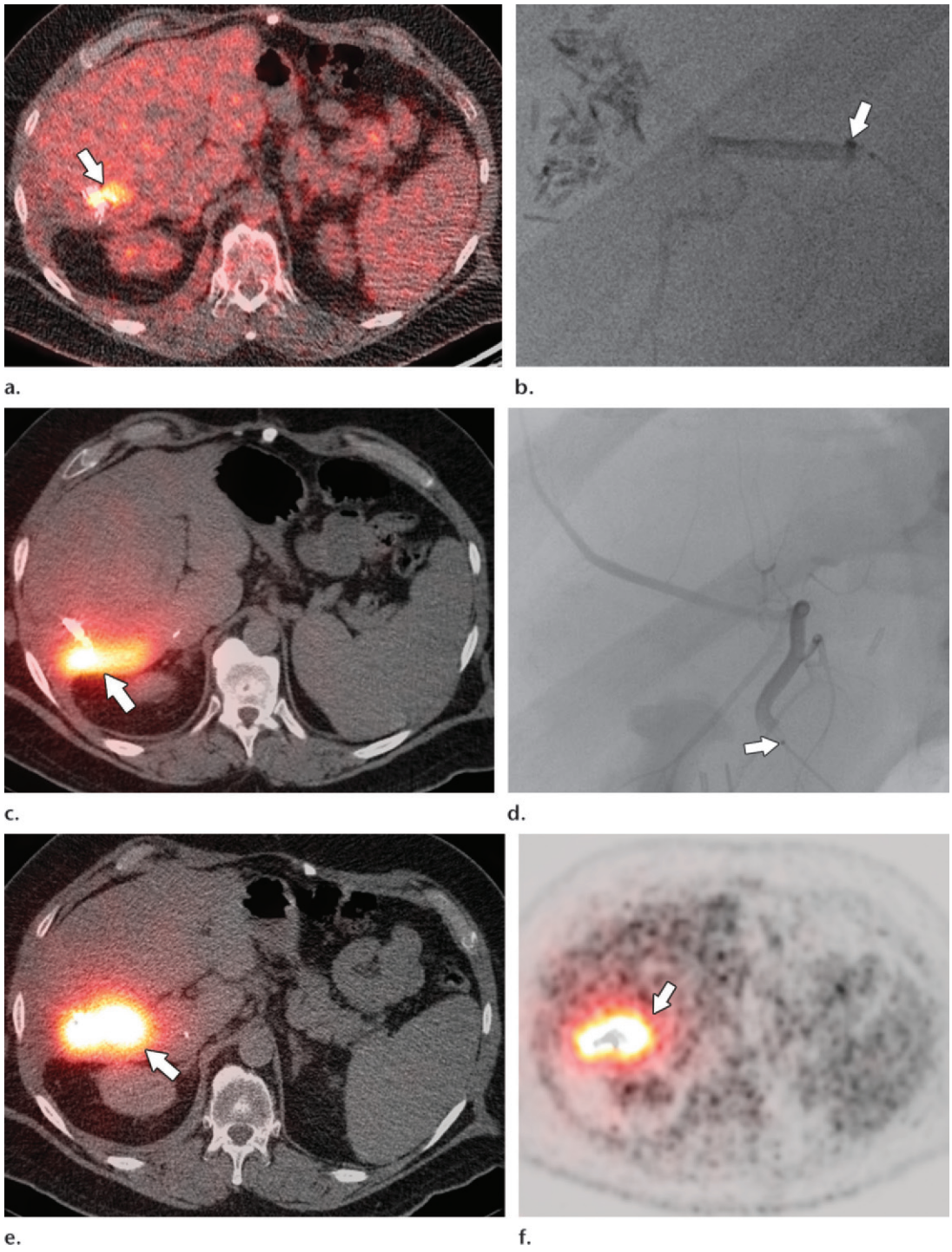

Figure 8. Initially incomplete target distribution, followed by complete distribution pattern. Images of a 48-year-old man with metastatic colorectal carcinoma show incomplete tumoral distribution at initial ^{90}Y microsphere therapy, a finding that was corrected with angiographic adjustment at subsequent therapy. **(a)** Coregistered axial FDG PET and CT image shows an FDG-avid lesion (arrow) within segment VI of the liver parenchyma adjacent to a prior resection margin, a finding that corresponds to metastatic disease. **(b)** Selective angiogram of the posterior and inferior branch of the right hepatic artery (arrow) shows adequate catheter position for ^{90}Y microsphere delivery. **(c)** Coregistered axial ^{90}Y bremsstrahlung and SPECT/CT image shows incomplete tumoral distribution of the ^{90}Y microspheres (arrow), which were deposited in the posterior margin of the parenchyma, partially treating the metabolically active tumor. **(d)** Subsequent selective angiogram shows identification of an additional branch of the superior division within the posterior right hepatic artery (arrow) that was supplying the target lesion, and therefore the catheter was repositioned for ^{90}Y microsphere delivery. **(e)** Coregistered axial ^{90}Y bremsstrahlung and SPECT/CT image shows the now complete tumoral distribution of the ^{90}Y microspheres (arrow), which are targeting the metabolically active tumor burden. **(f)** Coregistered axial posttherapy ^{90}Y bremsstrahlung and pretherapy FDG PET image shows complete tumoral ^{90}Y microsphere distribution (arrow), as manifested by FDG activity (black) within the treatment field (orange).

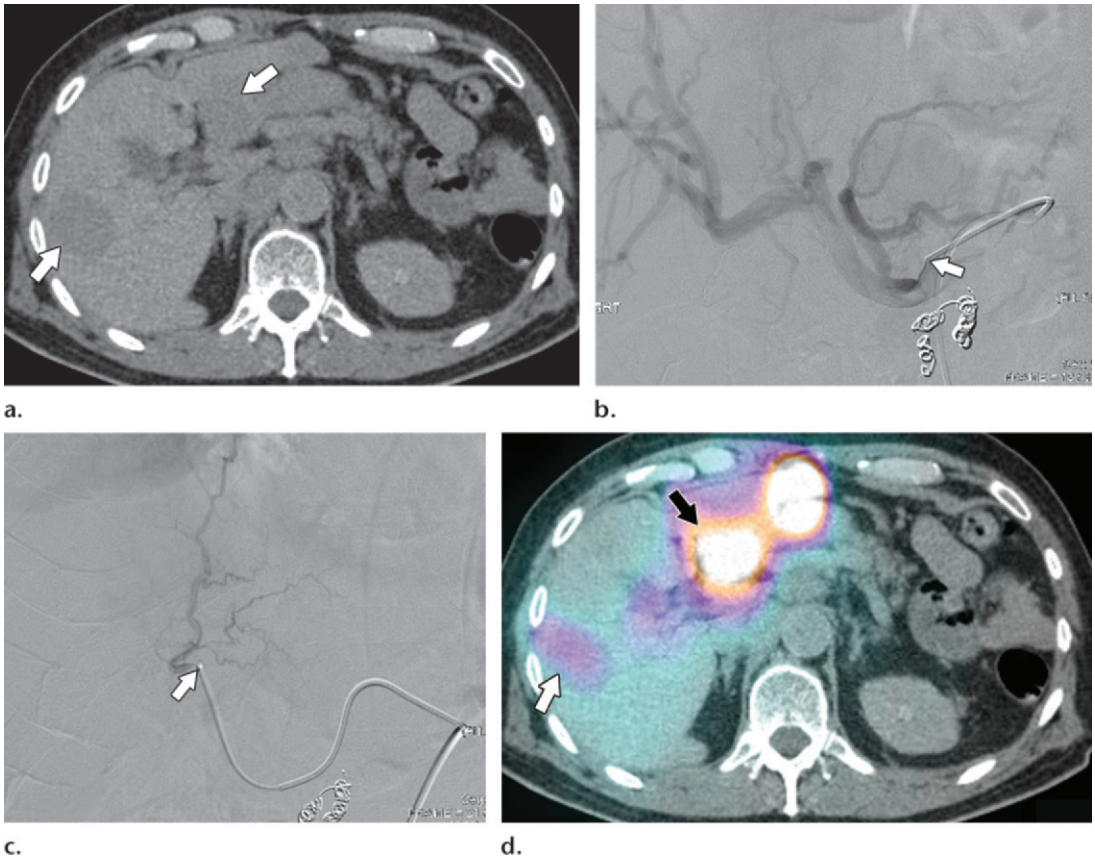

Figure 9. Complete target intratumoral distribution and also nontarget intrahepatic distribution. Images of a 69-year-old woman undergoing ^{90}Y microsphere therapy for a metastatic neuroendocrine tumor show nontarget intrahepatic particle redistribution. **(a)** Axial nonenhanced CT image shows bilateral multifocal hypoattenuating liver lesions (arrows), findings that correspond with known neuroendocrine tumor metastases. **(b)** Angiogram obtained before ^{90}Y microsphere therapy from the common hepatic artery (arrow) shows conventional hepatic anatomy. **(c)** Angiogram obtained at the time of therapy shows that the catheter was selectively placed into the left hepatic artery (arrow) to treat the majority of the tumor burden, which was located in the left hepatic lobe. **(d)** Axial ^{90}Y bremsstrahlung SPECT/CT image obtained after treatment shows that although complete tumoral distribution of the therapy (black arrow) was depicted, the right hepatic lobe also showed ^{90}Y microsphere activity, which fortuitously was deposited into the dominant segment V lesion (white arrow), likely because of preferential increased arterial flow through intrahepatic shunting at a capillary level.

goal is to treat the tumor burden with the least effect on the normal parenchyma. Unintended liver embolization is usually related to preferential increased arterial flow through intrahepatic shunting at a capillary level or microsphere reflux into nontarget vessels (Fig 9).

When nontarget extrahepatic activity is identified, it is usually related to the presence of flow collateralization by either parasitizing or normal vessels and may be avoidable by repositioning the catheter (Fig 10). Nontarget embolization includes involvement of the stomach, bowel, mesentery, gallbladder, pancreas, and, potentially, the umbilical region (Fig 11). Extrahepatic nontarget flow to the umbilical region may be difficult to detect because of vessel size and may require an extended injection for proper identification. In addition, reviewing the ^{99m}Tc-MAA examination with a range of windowing may allow detection of subtle activity in the umbilical artery region.

Although most vessels are identified at conventional angiography, sometimes the caliber of these structures is too small for adequate detection, and nontarget extrahepatic embolization may then occur despite optimal therapy administration technique and lack of visualization at pretherapy ^{99m}Tc-MAA SPECT/CT imaging. However, in these instances, the extrahepatic deposition will be detected at posttherapy ^{90}Y bremsstrahlung SPECT/CT or PET/CT, and appropriate action may be taken, including close observation or administration of prophylactic medication (Fig 12).

Conclusion

^{90}Y microsphere therapy is a complex procedure that relies on the principle of intraarterial brachytherapy and requires a multidisciplinary team approach combining expertise in cross-sectional imaging, nuclear medicine, and flow dynamics to adequately target patient tumor burden and to

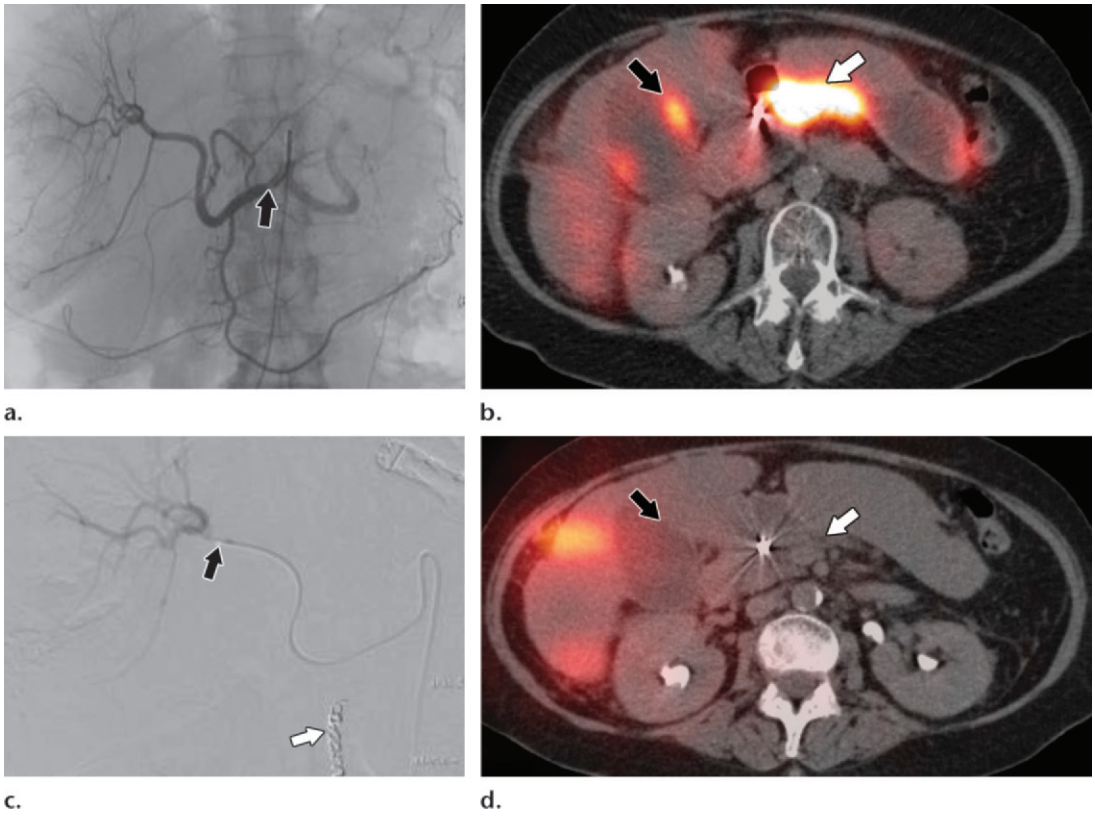

Figure 10. Nontarget extrahepatic distribution at pretherapy imaging avoided at therapy. Images of a 67-year-old woman with metastatic colon cancer show ^{90}Y nontarget distribution, with initial ^{99m}Tc-MAA SPECT/CT demonstrating gallbladder and gastroduodenal activity, which was avoided at subsequent therapy delivery. **(a)** Common hepatic angiogram obtained before ^{99m}Tc-MAA SPECT/CT shows conventional anatomy, with no replaced or accessory hepatic artery. At this time, coil embolization of the gastroduodenal artery was performed (not shown), and ^{99m}Tc-MAA injection was performed from the proper hepatic artery (arrow). **(b)** Axial ^{99m}Tc-MAA SPECT/CT image shows intense extrahepatic uptake in the gallbladder wall (black arrow) and the distal stomach and proximal duodenum (white arrow). **(c)** Angiogram shows that with selective placement of the catheter into the right hepatic artery, distal to the origin of the cystic artery and the right gastric artery (black arrow), and with coil embolization of the gastroduodenal artery (white arrow), nontarget distribution was avoided. **(d)** Axial ^{90}Y bremsstrahlung SPECT/CT image shows the expected uptake in the right hepatic lobe, with no gallbladder wall uptake (black arrow) and no gastroduodenal uptake (white arrow).

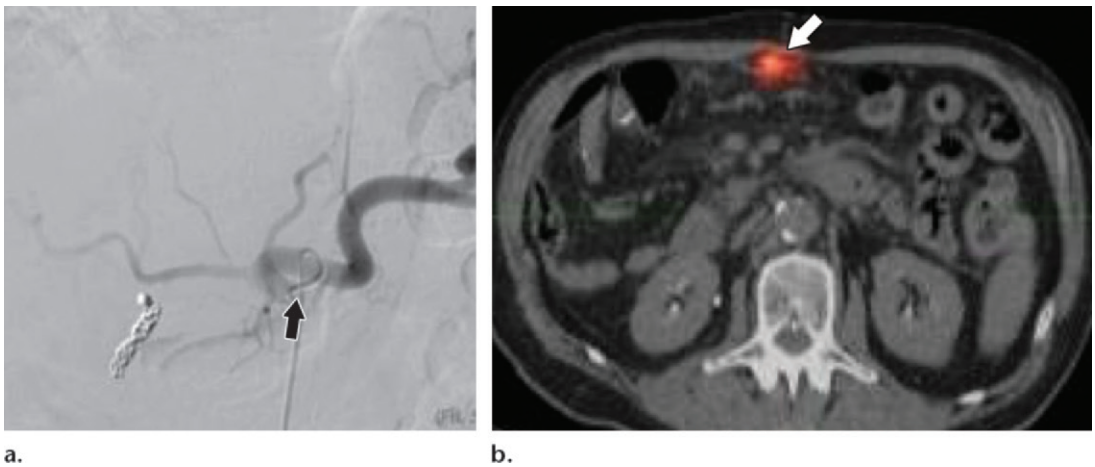

Figure 11. Nontarget extrahepatic distribution. Images of a 58-year-old man with metastatic colon cancer show ^{90}Y nontarget distribution, with initial ^{99m}Tc-MAA SPECT/CT demonstrating umbilical activity, which was not avoided at subsequent therapy delivery. **(a)** Angiogram of the celiac trunk (arrow) obtained before ^{99m}Tc-MAA SPECT/CT after coil embolization of the gastroduodenal artery shows conventional anatomy without an apparent umbilical artery. **(b)** Axial ^{99m}Tc-MAA SPECT/CT image shows subtle midline abdominal uptake (arrow) extending to the level of the umbilicus, a finding that was visible only in retrospect with narrow windowing. *(Figure 11 continues.)*

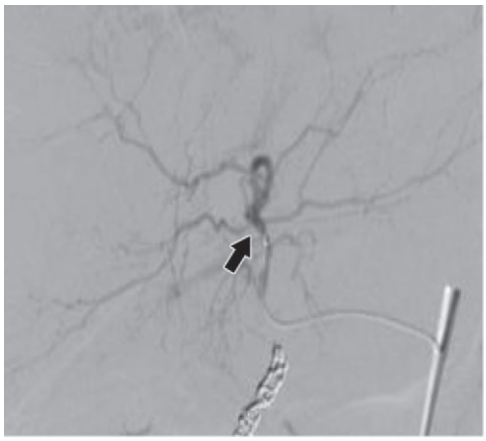

c.

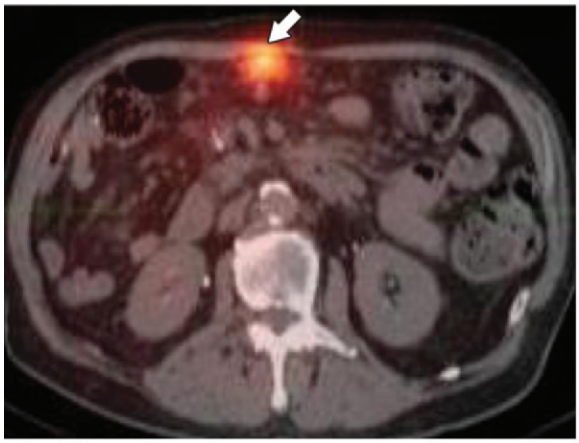

d.

e.

Figure 11. *(continued)* **(c)** Angiogram shows that the left hepatic lobe was treated with selective placement of the catheter into the left hepatic artery (arrow). **(d)** Axial ^{90}Y bremsstrahlung SPECT/CT image shows intense uptake extending to the umbilicus (arrow). **(e)** Photograph shows that the patient subsequently developed a grade 1 topical radiation injury (arrow), which was treated conservatively and later formed granulation tissue and resolved.

achieve optimal oncologic outcomes. In addition, a multimodality imaging pattern approach is useful to avoid or anticipate possible complications, to ensure adequate microsphere distribution, and to plan subsequent therapeutic interventions.

Acknowledgments.—The location of the study, the facilities, and the study subjects were recruited at Emory University Affiliated Hospitals, Atlanta, Georgia. The authors express special thanks to Kevin J. Makowski, RBP, for the final figure editing.

References

1. Kooby DA, Egnatashvili V, Srinivasan S, et al. Comparison of yttrium-90 radioembolization and transcatheter arterial chemoembolization for the treatment of unresectable hepatocellular carcinoma. J Vasc Interv Radiol 2010; 21(2):224–230.
2. Sato KT, Lewandowski RJ, Mulcahy MF, et al. Unresectable chemorefractory liver metastases: radioembolization with ^{90}Y microspheres—safety, efficacy, and survival. Radiology 2008;247(2):507–515.
3. Vyleta M, Coldwell D. Radioembolization in the treatment of neuroendocrine tumor metastases to the liver. Int J Hepatol 2011;2011:785315. http://www.hindawi.com/journals/ijh/2011/785315/. Published December 22, 2011. Accessed July 7, 2015.
4. Xing M, Kokabi N, Camacho JC, Kooby DA, El-Rayes BF, Kim HS. ^{90}Y radioembolization versus chemoembolization in the treatment of hepatocellular carcinoma: an analysis of comparative effectiveness. J Comp Eff Res 2013; 2(4):435–444.
5. Xing M, Prajapati HJ, Dhanasekaran R, et al. Selective internal yttrium-90 radioembolization therapy (^{90}Y-SIRT) versus best supportive care in patients with unresectable metastatic melanoma to the liver refractory to systemic therapy: safety and efficacy cohort study. Am J Clin Oncol 2014 Aug 7. http://journals.lww.com/amjclinicaloncology/pages/articleviewer.aspx?year=9000&issue=00000&article=99224&type=abstract. Updated August 7, 2014. Accessed July 7, 2015.
6. Georgiades CS Sr, Geschwind JF. Radioactive microspheres for the treatment of HCC. In: Golzarian J, Sun S, Sharafuddin MJ, eds. Vascular embolotherapy: a comprehensive approach. New York, NY: Springer, 2005; 141–148.
7. Murthy R, Nunez R, Szklaruk J, et al. Yttrium-90 microsphere therapy for hepatic malignancy: devices, indications, technical considerations, and potential complications. RadioGraphics 2005;25(suppl 1):S41–S55.
8. Lau WY, Ho S, Leung TW, et al. Selective internal radiation therapy for nonresectable hepatocellular carcinoma with intraarterial infusion of ^{90}yttrium microspheres. Int J Radiat Oncol Biol Phys 1998;40(3):583–592.
9. Dawson LA, McGinn CJ, Normolle D, et al. Escalated focal liver radiation and concurrent hepatic artery fluorodeoxyuridine for unresectable intrahepatic malignancies. J Clin Oncol 2000;18(11):2210–2218.
10. Emami B, Lyman J, Brown A, et al. Tolerance of normal tissue to therapeutic irradiation. Int J Radiat Oncol Biol Phys 1991;21(1):109–122.
11. Ackerman NB, Lien WM, Kondi ES, Silverman NA. The blood supply of experimental liver metastases. I. The distribution of hepatic artery and portal vein blood to "small" and "large" tumors. Surgery 1969;66(6):1067–1072.
12. Dezarn WA, Cessna JT, DeWerd LA, et al. Recommendations of the American Association of Physicists in Medicine on dosimetry, imaging, and quality assurance procedures for

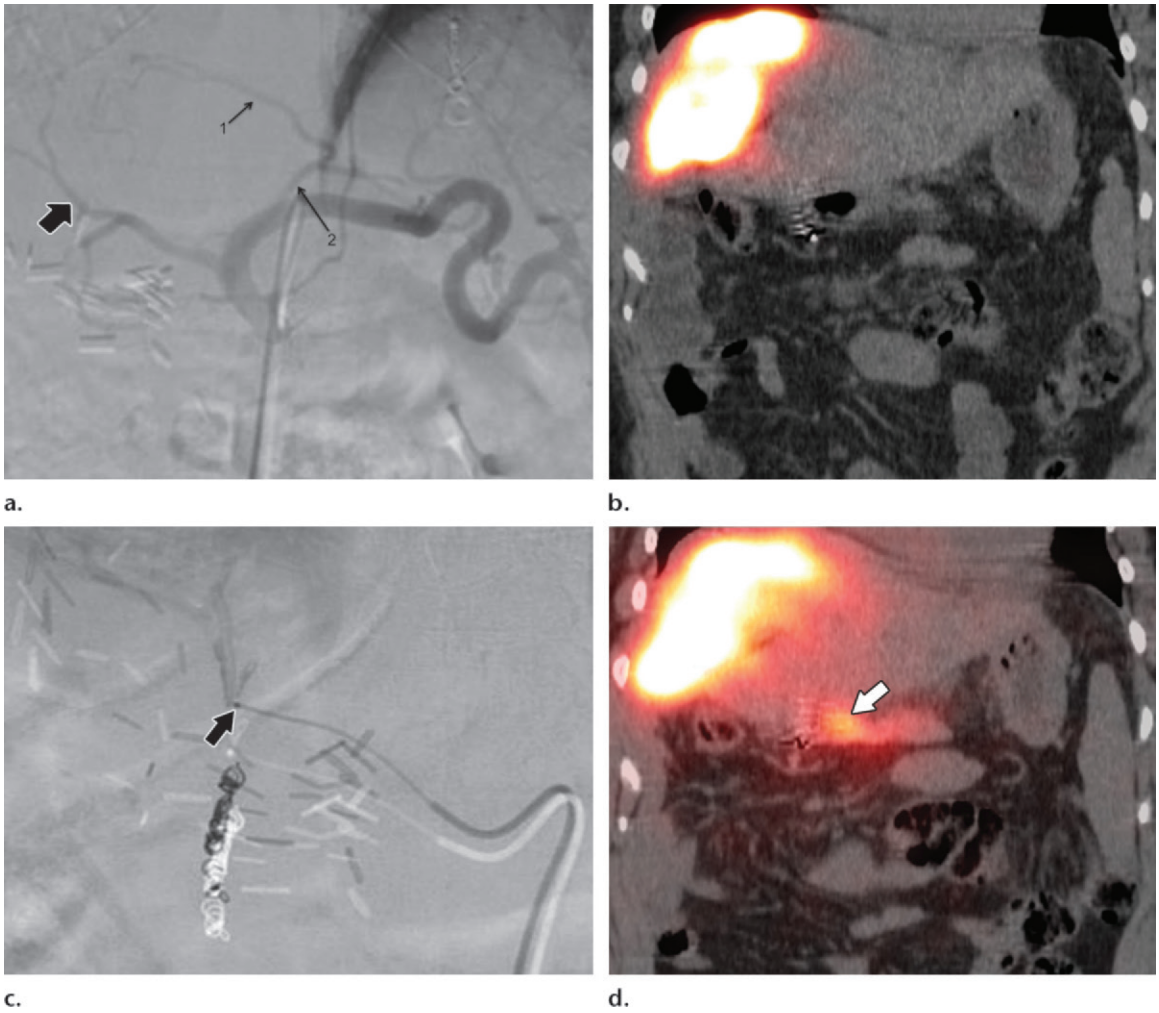

Figure 12. Nontarget extrahepatic distribution. Images of a 49-year-old woman with metastatic colon cancer who was undergoing treatment evaluation show no extrahepatic activity at initial ^{99m}Tc-MAA SPECT/CT but do show extrahepatic activity at postprocedural ^{90}Y bremsstrahlung SPECT/CT. **(a)** Angiogram obtained before ^{99m}Tc-MAA SPECT/CT shows an accessory left hepatic artery *(1)* originating from the left gastric artery *(2)*. Postsurgical changes from a prior right hepatectomy are depicted, with a normal appearance of the left hepatic artery (thick arrow). **(b)** Coronal ^{99m}Tc-MAA SPECT/CT image shows no evidence of extrahepatic uptake. Segment IV was the only region being treated in this session (right lateral anatomic position was due to right hepatectomy). **(c)** Angiogram obtained at treatment shows selective placement of the catheter into the left hepatic artery (arrow). Note coil embolization of the gastroduodenal artery. **(d)** Coronal ^{90}Y bremsstrahlung SPECT/CT image shows uptake within segment IV, but also in the proximal stomach (arrow), probably through flow redistribution to a small right gastric artery after embolization of the gastroduodenal artery. The patient was subsequently treated conservatively with sucralfate and did not develop complications.

^{90}Y microsphere brachytherapy in the treatment of hepatic malignancies. Med Phys 2011;38(8):4824–4845.
13. Salem R, Lewandowski RJ, Atassi B, et al. Treatment of unresectable hepatocellular carcinoma with use of ^{90}Y microspheres (TheraSphere): safety, tumor response, and survival. J Vasc Interv Radiol 2005;16(12):1627–1639.
14. Stubbs RS, Cannan RJ, Mitchell AW. Selective internal radiation therapy (SIRT) with ^{90}yttrium microspheres for extensive colorectal liver metastases. Hepatogastroenterology 2001;48(38):333–337.
15. Salem R, Thurston KG. Radioembolization with ^{90}yttrium microspheres: a state-of-the-art brachytherapy treatment for primary and secondary liver malignancies. I. Technical and methodologic considerations. J Vasc Interv Radiol 2006;17(8):1251–1278.
16. Grady ED. Intrahepatic arterial 90-yttrium resin spheres to treat liver cancer. Int J Nucl Med Biol 1978;5(6):253–254.
17. Andrews JC, Walker SC, Ackermann RJ, Cotton LA, Ensminger WD, Shapiro B. Hepatic radioembolization with yttrium-90 containing glass microspheres: preliminary results and clinical follow-up. J Nucl Med 1994;35(10):1637–1644.
18. TheraSphere [package insert]. Ottawa, Ontario: Nordion (Canada) Inc for BTG International, 2012.
19. Geschwind JF, Salem R, Carr BI, et al. Yttrium-90 microspheres for the treatment of hepatocellular carcinoma. Gastroenterology 2004;127(5 suppl 1):S194–S205.
20. Lewandowski RJ, Salem R. Yttrium-90 radioembolization of hepatocellular carcinoma and metastatic disease to the liver. Semin Intervent Radiol 2006;23(1):64–72.
21. Chow PK, Poon DY, Khin MW, et al. Multicenter phase II study of sequential radioembolization-sorafenib therapy for inoperable hepatocellular carcinoma. PLoS ONE 2014;9(3):e90909. http://journals.plos.org/plosone/article?id=10.1371/journal.pone.0090909.Accessed July 7, 2015.
22. Hilgard P, Hamami M, Fouly AE, et al. Radioembolization with yttrium-90 glass microspheres in hepatocellular carcinoma: European experience on safety and long-term survival. Hepatology 2010;52(5):1741–1749.

23. Lambert B, Sturm E, Mertens J, et al. Intra-arterial treatment with ^{90}Y microspheres for hepatocellular carcinoma: 4 years experience at the Ghent University Hospital. Eur J Nucl Med Mol Imaging 2011;38(12):2117–2124.
24. Mazzaferro V, Sposito C, Bhoori S, et al. Yttrium-90 radioembolization for intermediate-advanced hepatocellular carcinoma: a phase 2 study. Hepatology 2013;57(5):1826–1837.
25. Lewandowski RJ, Thurston KG, Goin JE, et al. ^{90}Y microsphere (TheraSphere) treatment for unresectable colorectal cancer metastases of the liver: response to treatment at targeted doses of 135-150 Gy as measured by [18F]fluorodeoxyglucose positron emission tomography and computed tomographic imaging. J Vasc Interv Radiol 2005;16(12):1641–1651.
26. Kennedy A, Nag S, Salem R, et al. Recommendations for radioembolization of hepatic malignancies using yttrium-90 microsphere brachytherapy: a consensus panel report from the Radioembolization Brachytherapy Oncology Consortium. Int J Radiat Oncol Biol Phys 2007;68(1):13–23.
27. Haug AR, Heinemann V, Bruns CJ, et al. ^{18}F-FDG PET independently predicts survival in patients with cholangiocellular carcinoma treated with ^{90}Y microspheres. Eur J Nucl Med Mol Imaging 2011;38(6):1037–1045.
28. Szyszko T, Al-Nahhas A, Canelo R, et al. Assessment of response to treatment of unresectable liver tumours with ^{90}Y microspheres: value of FDG PET versus computed tomography. Nucl Med Commun 2007;28(1):15–20.
29. Wong CY, Salem R, Raman S, Gates VL, Dworkin HJ. Evaluating ^{90}Y-glass microsphere treatment response of unresectable colorectal liver metastases by [^{18}F]FDG PET: a comparison with CT or MRI. Eur J Nucl Med Mol Imaging 2002;29(6):815–820.
30. Rafi S, Piduru SM, El-Rayes B, et al. Yttrium-90 radioembolization for unresectable standard-chemorefractory intrahepatic cholangiocarcinoma: survival, efficacy, and safety study. Cardiovasc Intervent Radiol 2013;36(2):440–448.
31. Saxena A, Bester L, Shan L, et al. A systematic review on the safety and efficacy of yttrium-90 radioembolization for unresectable, chemorefractory colorectal cancer liver metastases. J Cancer Res Clin Oncol 2014;140(4):537–547.
32. Lewandowski RJ, Sato KT, Atassi B, et al. Radioembolization with ^{90}Y microspheres: angiographic and technical considerations. Cardiovasc Intervent Radiol 2007;30(4):571–592.
33. Hiatt JR, Gabbay J, Busuttil RW. Surgical anatomy of the hepatic arteries in 1000 cases. Ann Surg 1994;220(1):50–52.
34. Michels NA. Newer anatomy of the liver and its variant blood supply and collateral circulation. Am J Surg 1966;112(3):337–347.
35. Liu DM, Salem R, Bui JT, et al. Angiographic considerations in patients undergoing liver-directed therapy. J Vasc Interv Radiol 2005;16(7):911–935.
36. Abdelmaksoud MH, Louie JD, Kothary N, et al. Consolidation of hepatic arterial inflow by embolization of variant hepatic arteries in preparation for yttrium-90 radioembolization. J Vasc Interv Radiol 2011;22(10):1364–1371, e1.
37. Campbell AM, Bailey IH, Burton MA. Analysis of the distribution of intra-arterial microspheres in human liver following hepatic yttrium-90 microsphere therapy. Phys Med Biol 2000;45(4):1023–1033.
38. Karunanithy N, Gordon F, Hodolic M, et al. Embolization of hepatic arterial branches to simplify hepatic blood flow before yttrium 90 radioembolization: a useful technique in the presence of challenging anatomy. Cardiovasc Intervent Radiol 2011;34(2):287–294.
39. Lambert B, Mertens J, Sturm EJ, Stienaers S, Defreyne L, D'Asseler Y. ^{99m}Tc-labelled macroaggregated albumin (MAA) scintigraphy for planning treatment with ^{90}Y microspheres. Eur J Nucl Med Mol Imaging 2010;37(12):2328–2333.
40. Kowalsky RJ, Falen SW. Radiopharmaceuticals in nuclear pharmacy and nuclear medicine. 2nd ed. Forrester Center, WVa: American Pharmacists Association, 2004.
41. Dancey JE, Shepherd FA, Paul K, et al. Treatment of nonresectable hepatocellular carcinoma with intrahepatic ^{90}Y-microspheres. J Nucl Med 2000;41(10):1673–1681.
42. Jakobs TF, Hoffmann RT, Poepperl G, et al. Mid-term results in otherwise treatment refractory primary or secondary liver confined tumours treated with selective internal radiation therapy (SIRT) using (90)yttrium resin-microspheres. Eur Radiol 2007;17(5):1320–1330.
43. Jiao LR, Szyszko T, Al-Nahhas A, et al. Clinical and imaging experience with yttrium-90 microspheres in the management of unresectable liver tumours. Eur J Surg Oncol 2007;33(5):597–602.
44. Leung TW, Lau WY, Ho SK, et al. Radiation pneumonitis after selective internal radiation treatment with intraarterial ^{90}yttrium-microspheres for inoperable hepatic tumors. Int J Radiat Oncol Biol Phys 1995;33(4):919–924.
45. Ahmadzadehfar H, Sabet A, Biermann K, et al. The significance of ^{99m}Tc-MAA SPECT/CT liver perfusion imaging in treatment planning for ^{90}Y-microsphere selective internal radiation treatment. J Nucl Med 2010;51(8):1206–1212.
46. Ahmadzadehfar H, Sabet A, Muckle M, et al. ^{99m}Tc-MAA/^{90}Y-Bremsstrahlung SPECT/CT after simultaneous Tc-MAA/^{90}Y-microsphere injection for immediate treatment monitoring and further therapy planning for radioembolization. Eur J Nucl Med Mol Imaging 2011;38(7):1281–1288.
47. Brandon D, Alazraki A, Halkar RK, Alazraki NP. The role of single-photon emission computed tomography and SPECT/computed tomography in oncologic imaging. Semin Oncol 2011;38(1):87–108.
48. Hamami ME, Poeppel TD, Müller S, et al. SPECT/CT with ^{99m}Tc-MAA in radioembolization with ^{90}Y microspheres in patients with hepatocellular cancer. J Nucl Med 2009;50(5):688–692.
49. Heusner TA, Hamami ME, Ertle J, et al. Angiography-based C-arm CT for the assessment of extrahepatic shunting before radioembolization. Rofo 2010;182(7):603–608.
50. Murthy R, Mutha P, Madoff DC, Mahvash A, Erwin W. Establishment of the radiation effect of yttrium-90 microspheres: role of C-arm CT. J Vasc Interv Radiol 2009;20(3):422–424.
51. Louie JD, Kothary N, Kuo WT, et al. Incorporating cone-beam CT into the treatment planning for yttrium-90 radioembolization. J Vasc Interv Radiol 2009;20(5):606–613.
52. Becker C, Waggershauser T, Tiling R, et al. C-arm computed tomography compared with positron emission tomography/computed tomography for treatment planning before radioembolization. Cardiovasc Intervent Radiol 2011;34(3):550–556.
53. SIR-Spheres microspheres [package insert]. North Sydney, Australia: Sirtex Medical. http://www.sirtex.com/media/8163/pi-ec-11.pdf. Published December 2013. Accessed July 7, 2015.
54. Kokabi N, Galt JR, Xing M, et al. A simple method for estimating dose delivered to hepatocellular carcinoma after yttrium-90 glass-based radioembolization therapy: preliminary results of a proof of concept study. J Vasc Interv Radiol 2014;25(2):277–287.
55. Kao YH, Hock Tan AE, Burgmans MC, et al. Image-guided personalized predictive dosimetry by artery-specific SPECT/CT partition modeling for safe and effective ^{90}Y radioembolization. J Nucl Med 2012;53(4):559–566.
56. Dieudonné A, Garin E, Laffont S, et al. Clinical feasibility of fast 3-dimensional dosimetry of the liver for treatment planning of hepatocellular carcinoma with ^{90}Y-microspheres. J Nucl Med 2011;52(12):1930–1937.
57. Ulrich G, Dudeck O, Furth C, et al. Predictive value of intratumoral ^{99m}Tc-macroaggregated albumin uptake in patients with colorectal liver metastases scheduled for radioembolization with ^{90}Y-microspheres. J Nucl Med 2013;54(4):516–522.
58. Wondergem M, Smits ML, Elschot M, et al. ^{99m}Tc-macroaggregated albumin poorly predicts the intrahepatic distribution of ^{90}Y resin microspheres in hepatic radioembolization. J Nucl Med 2013;54(8):1294–1301.
59. Ahmadzadehfar H, Duan H, Haug AR, Walrand S, Hoffmann M. The role of SPECT/CT in radioembolization of liver tumours. Eur J Nucl Med Mol Imaging 2014;41(suppl 1):S115–S124.
60. Mansberg R, Sorensen N, Mansberg V, Van der Wall H. Yttrium 90 bremsstrahlung SPECT/CT scan demonstrating areas of tracer/tumour uptake. Eur J Nucl Med Mol Imaging 2007;34(11):1887. http://link.springer.com/article/10.1007%2Fs00259-007-0536-9. Published September 11, 2007. Accessed July 7, 2015.

61. Barber TW, Yap KS, Cherk MH, Powell A, Kalff V. Comparison of positron emission tomography/CT and bremsstrahlung imaging following Y-90 radiation synovectomy. J Med Imaging Radiat Oncol 2013;57(5):567–571.
62. Elschot M, Vermolen BJ, Lam MG, de Keizer B, van den Bosch MA, de Jong HW. Quantitative comparison of PET and bremsstrahlung SPECT for imaging the in vivo yttrium-90 microsphere distribution after liver radioembolization. PLoS ONE 2013;8(2):e55742. http://journals.plos.org/plosone/article?id=10.1371/journal.pone.0055742. Published February 6, 2013. Accessed July 7, 2015.
63. Garin E, Lenoir L, Rolland Y, et al. Dosimetry based on ^{99m}Tc-macroaggregated albumin SPECT/CT accurately predicts tumor response and survival in hepatocellular carcinoma patients treated with ^{90}Y-loaded glass microspheres: preliminary results. J Nucl Med 2012;53(2):255–263.
64. Kao YH, Tan EH, Ng CE, Goh SW. Yttrium-90 time-of-flight PET/CT is superior to bremsstrahlung SPECT/CT for postradioembolization imaging of microsphere biodistribution. Clin Nucl Med 2011;36(12):e186–e187.
65. Padia SA, Alessio A, Kwan SW, Lewis DH, Vaidya S, Minoshima S. Comparison of positron emission tomography and bremsstrahlung imaging to detect particle distribution in patients undergoing yttrium-90 radioembolization for large hepatocellular carcinomas or associated portal vein thrombosis. J Vasc Interv Radiol 2013;24(8):1147–1153.
66. Gates VL, Salem R, Lewandowski RJ. Positron emission tomography/CT after yttrium-90 radioembolization: current and future applications. J Vasc Interv Radiol 2013;24(8):1153–1155.

This journal-based SA-CME activity has been approved for ***AMA PRA Category 1 Credit™****. See www.rsna.org/education/search/RG.*